J. Fluid Mech. (1978), *vol.* 85, *part* 3, *pp.* 417–431
Printed in Great Britain

Experiments on strong interactions between solitary waves

By P. D. WEIDMAN AND T. MAXWORTHY

Department of Aerospace Engineering, University of Southern California, Los Angeles

(Received 11 May 1976 and in revised form 9 May 1977)

Experiments on the interaction between solitary shallow-water waves propagating in the same direction have been performed in a rectangular channel. Two methods were devised to compensate for the dissipation of the waves in order to compare results with Hirota's (1971) solution for the collision of solitons described by the Korteweg–de Vries equation. Both qualitative and quantitative agreement with theory is obtained using the proposed corrections for wave damping.

1. Introduction

In Maxworthy (1976), where we were concerned with *weakly*† interacting solitary waves, the measurements reported were in qualitative agreement with the analyses of Byatt-Smith (1971) and Oikawa & Yajima (1973) in that the waves experienced a backward shift and the maximum wave amplitude during interaction was greater than twice that of the initial waves. The major quantitative difference between theory and experiment was in the magnitude of the spatial phase shift; whereas the theories give a square-root dependence on wave amplitude, the measurements indicated a nearly constant spatial phase shift ($\Delta X/h_0 \simeq -1{\cdot}2$) over a substantial range of amplitudes ($0{\cdot}1 < \eta/h_0 < 0{\cdot}45$). This led to the suggestion that the pair of Boussinesq equations (see Byatt-Smith 1971, equations (1.2) and (1.3), for example) used to model the interaction were inadequate as a description of the large vertical accelerations observed.

In this paper we report on measurements of the *strong*† interaction which takes place when one solitary wave overtakes another of smaller amplitude travelling in the same direction. We now suspect that the Boussinesq equations are likely to be valid and, in this case, they reduce to the unidirectional Korteweg–de Vries (KdV) equation. Indeed, the careful measurements by Hammack & Segur (1974) on the evolution of solitary waves from a variety of initial displacements have verified the asymptotic behaviour predicted by the KdV equation. In particular, the number of solitons which evolved and their asymptotic wave forms were found to be in essential agreement with the nonlinear theory. The present study will be seen to complement their important work.

The exact solution of the KdV equation for multiple soliton collisions was first given by Hirota (1971) and is discussed in detail by Whitham (1974, pp. 580–585) for the case of an interaction between two waves. Prior to this, Lax (1968) had delineated

† We adopt the adjectives *weak* and *strong* introduced by Miles (1977*b*) to differentiate between the short-time interaction of solitons colliding head-on and the long-time interaction between solitons travelling in the same direction.

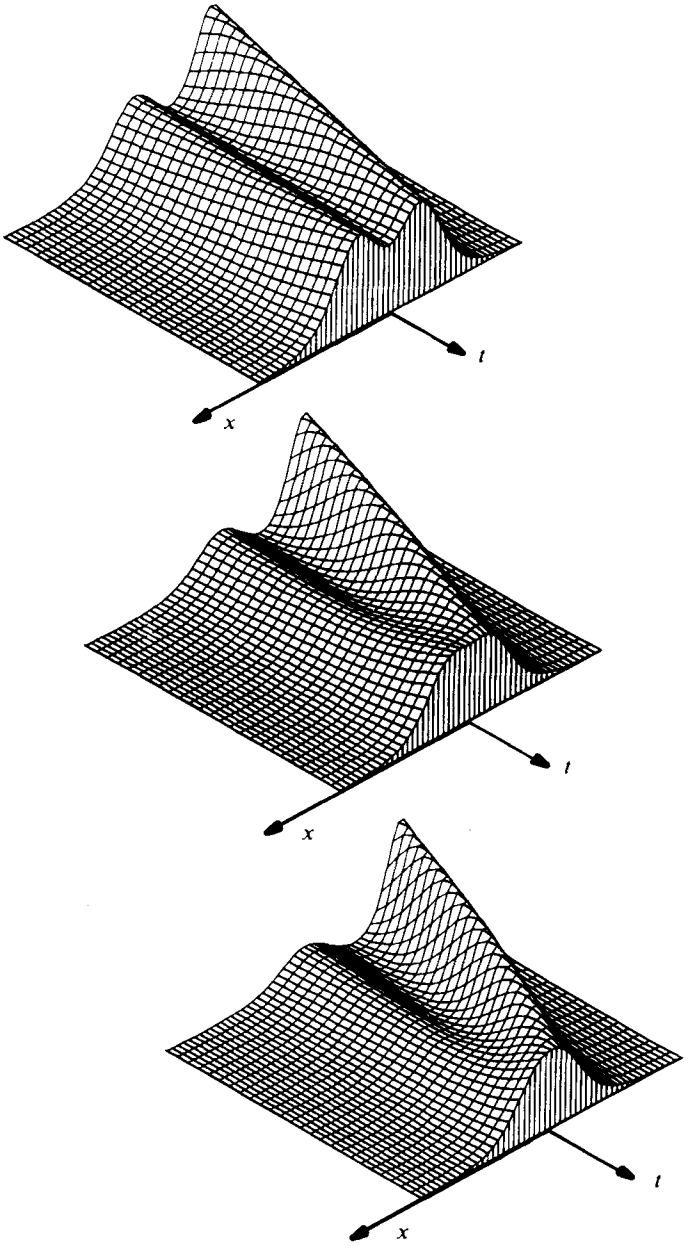

(a) $1 < \sigma < \frac{1}{2}(3+5^{\frac{1}{2}})$

(b) $\frac{1}{2}(3+5^{\frac{1}{2}}) < \sigma < 3$

(c) $\sigma > 3$

FIGURE 1. Illustrations of the three types of KdV interaction according to Lax (1968).

the three possible types of KdV interaction, which he called classes (*a*), (*b*) and (*c*), a notation which we also employ. Each type of interaction is illustrated in figure 1, where we have plotted Hirota's (1971) solution up to the middle of the interaction, $t = 0$. The different cases can be classified according to the amplitude ratio $\sigma = \alpha_2/\alpha_1$, where α_1 and α_2 ($\alpha_2 > \alpha_1$) represent the dimensional wave amplitudes η_1 and η_2 normalized by the still-water depth h_0. Although the interaction phenomena have been described by several authors (for a particularly novel interpretation, see Kruskal

1974), Lax's class (*b*) is sometimes neglected. For the small range of relative amplitudes corresponding to this case, the faster wave tries to engulf the slower one, and in fact the small amplitude wave loses its crest only to regain it just prior to the middle of the interaction. The theory shows that in every case the larger wave experiences a forward shift while the smaller wave undergoes a backward shift as a result of the interaction. The purpose of the present investigation is to test these predictions experimentally.

The apparatus used to perform the experiment is described in § 2. In § 3 we discuss the problem of dissipation and propose two ways to account for it in order to estimate the non-dissipative phase shifts. The results, including mid-interaction amplitude measurements, are presented in § 4 and in § 5 we offer some concluding remarks.

2. Apparatus and data acquisition

The rectangular lucite channel (20 cm wide × 30 cm deep) used was essentially the one described by Maxworthy (1976) except that additional 1·75 m sections were added to provide a working length of more than 14 m. The channel could be levelled to within better than $\pm 2{\cdot}0$ mm over its entire length with the aid of adjustable screws supporting each section.

The single most essential improvement in the facility was the development of a piston-action wave maker, with controlling electronics designed to produce repeatable initial wave forms. The wave maker, sketched in figure 2, consisted of a rectangular Plexiglas piston mounted at one end of a stainless-steel shaft guided by two split linear bearings mounted on an extension of the last channel section. A geared rack was inlaid along the top of the shaft so that it moved in the split of the linear bearings, and the system was driven by a reversible 12 V d.c. motor via a pinion that engaged the rack. Weather-stripping provided a flexible seal for the piston and a Teflon film coating the channel walls in the driver section kept the frictional force on the plunger to a minimum.

The magnitude of the current applied to the motor determined the piston velocity, and an electronic circuit was designed to monitor the following features: (i) length of primary stroke; (ii) velocity of primary stroke; (iii) time delay between strokes; (iv) length of secondary stroke; (v) velocity of secondary stroke. A 10-turn potentiometer geared to the rack provided positioning information to the control circuit. With these controls alone, one could generate two square waves of velocity *vs.* time as depicted by the solid-line sketch above the piston in figure 2. Variable capacitors were included to control the rise and decay times of the current to the motor, thus providing a certain amount of wave shaping. The dashed-line velocity profile exhibits the modified piston action with this additional degree of freedom.

Position–time measurements of the wave crests were obtained photographically. To avoid parallax problems, a grid (0·5 × 2·0 cm) was prepared with waterproof ink on the inside wall of the channel over its entire length. A remotely controlled Nikon camera, triggered by a reed relay, was mounted on a trolley and pushed along beside the channel to follow the waves. The relay was fired by a pulse from a function generator and accurate time-interval measurements were obtained with a timer–counter. Tap water, used as the working medium, was dyed green in order to produce a sharp definition of the free surface along the side wall.

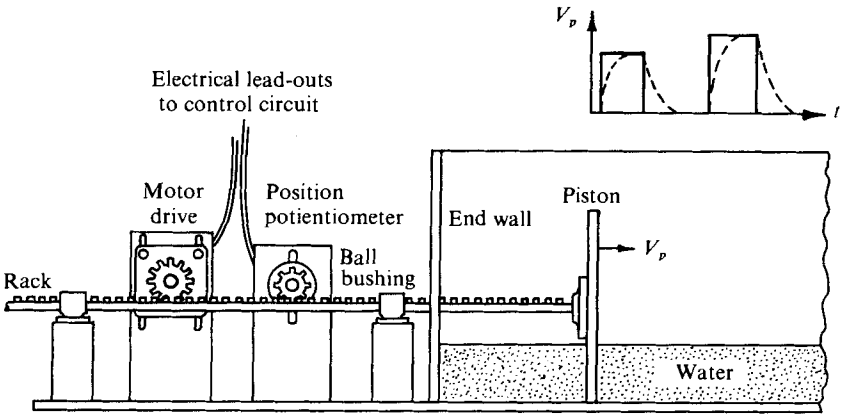

FIGURE 2. Diagram of the piston wave maker. The velocity history of the piston V_p is sketched for both the shaped (dashed line) and the unshaped (solid line) mode of operation.

3. Compensating for the effects of dissipation

After some initial experimentation, disturbances could be generated which rapidly evolved (after having travelled a distance of two wavelengths or less) into solitary waves followed by barely perceptible dispersive wave trains. These 'solitons', however, were subject to dissipation from various sources, and consequently the amplitude and speed of the waves diminished during their travel down the test section. Apart from the obvious source, that of viscous dissipation at the solid boundaries, small 'capillary' waves formed on the main wave crest at an oblique angle to the side walls and represented an additional loss of energy. These wavelets originated from hysteresis effects of the meniscus at the water–air–lucite contact line.

In figure 3 we compare typical amplitude attenuation measurements in our facility with Keulegan's (1948) theory for the damping of solitary waves propagating down a rectangular channel. The trend of our experimental data with the parameter η_0/h_0 is in accord with the theory, but we measured substantially greater attenuation. A discussion of this point and a comparison of our results with measurements reported in prior investigations is given in the appendix.

In order to extract estimates of the non-dissipative phase shifts, we have devised two means of correcting for the observed wave dissipation. The application of these compensation methods, described in the following two subsections, does not depend on the sources of dissipation, but assumes only that the dissipation takes place gradually and continuously along the channel. Furthermore, the two correction techniques can be used to check one against the other.

3.1. *Wave propagation in a channel of constant width*

Trajectories of typical large and small amplitude waves are plotted in figure 4 in an ξ, x plane, where $\xi = x - c_0 t$ and $c_0 = (gh_0)^{\frac{1}{2}}$ is the linear long-wave speed. The open and solid symbols represent data from two different runs and one can see that the reproducibility of the waves is good. The variable ξ is now a sensitive measure of nonlinear effects since we have subtracted out the distance travelled by a linear wave.

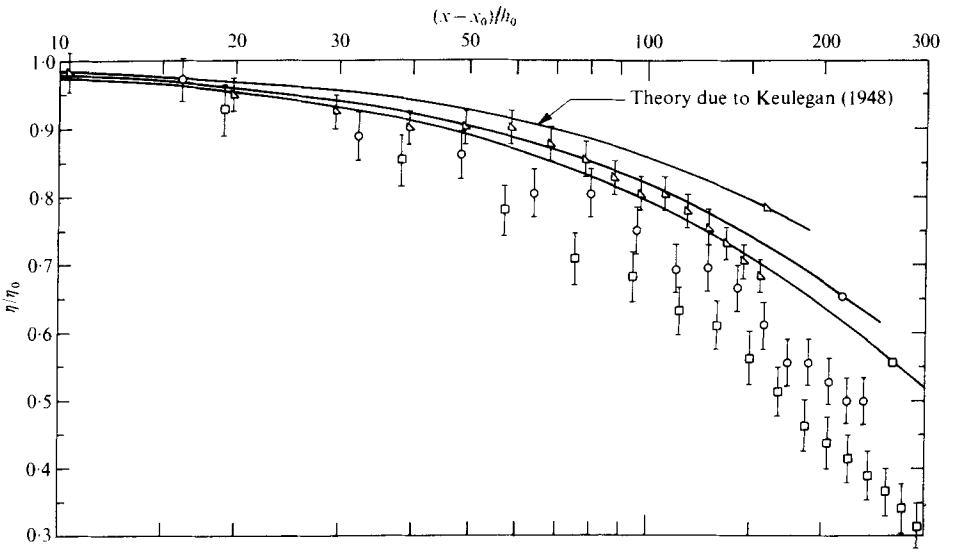

FIGURE 3. Amplitude attenuation of the solitary waves in the constant-width channel. ⊕, $\eta_0/h_0 = 0{\cdot}25$, $h_0 = 8{\cdot}1$ cm; ⊖, $\eta_0/h_0 = 0{\cdot}36$, $h_0 = 5{\cdot}0$ cm; ⊟, $\eta_0/h_0 = 0{\cdot}43$, $h_0 = 4{\cdot}0$ cm. The corresponding theoretical results due to Keulegan (1948) are also included.

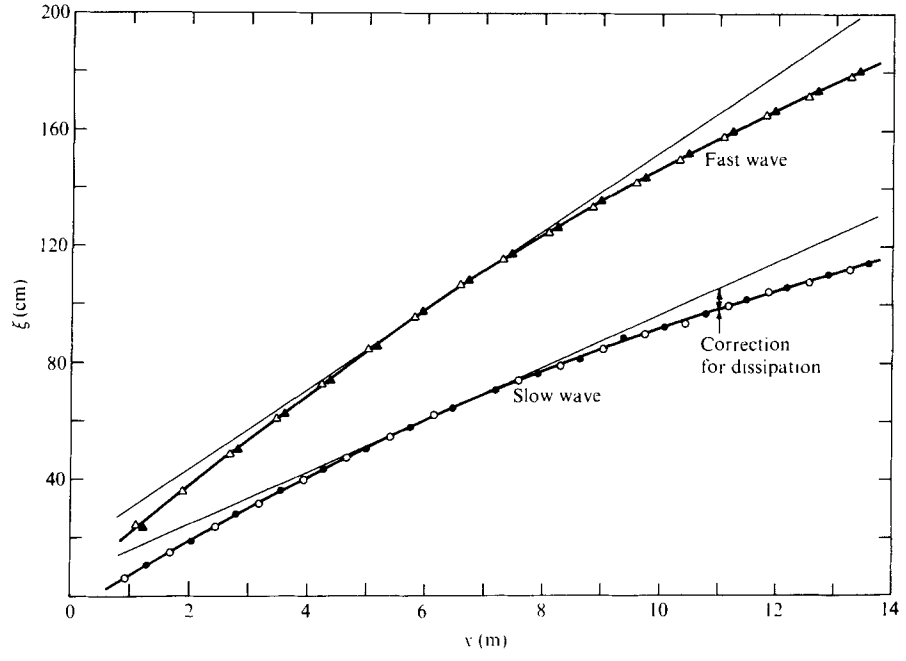

FIGURE 4. Non-interacting ξ, x trajectories of the primary (slow) and secondary (fast) waves produced by the wave maker in the constant-width channel. The open and solid symbols represent two separate runs. Tangents are drawn at $x = 6{\cdot}25$ m, corresponding to the interaction centre in figure 6, and a typical correction for dissipation is indicated.

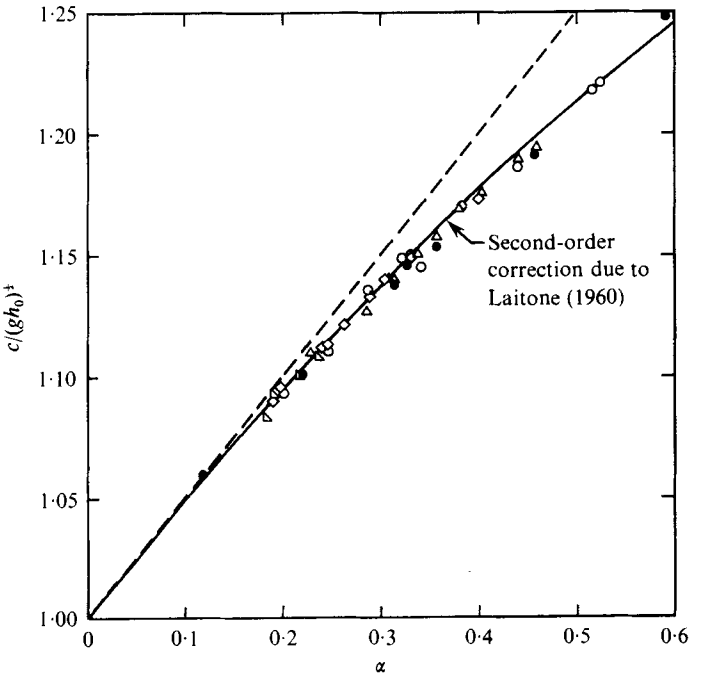

FIGURE 5. Wave speed as a function of amplitude. ○, ●, h_0 = 5·0 cm; △, h_0 = 6·0 cm; ◇, h_0 = 7·0 cm; ▷, h_0 = 8·1 cm. First- and second-order theoretical results due to Laitone (1960) are given by the dashed and solid curves respectively.

Moreover, the nonlinear wave speed $c(x)$ at each downstream position can be accurately calculated from the formula

$$c(x) = (gh_0)^{\frac{1}{2}}/(1-s(x)), \tag{3.1}$$

where $s(x)$ is the local slope of the trajectory. The measured variation of wave speed with wave amplitude is presented in figure 5. Henceforth measurements performed in the constant-width channel will be plotted as open symbols, while those obtained from the converging channel (to be discussed in § 3.2) will be plotted as solid circles. The amplitudes in figure 5 were taken from best-fit curves drawn through the measured data (e.g. figure 3) and the velocities were computed from (3.1) using the local measured trajectory slope. First- and second-order theoretical results for a solitary wave are given by the dashed and solid curves, respectively. We see that there is close agreement with Laitone's (1960) higher-order result

$$c = (gh_0)^{\frac{1}{2}}(1+\tfrac{1}{2}\alpha-\tfrac{3}{20}\alpha^2+\ldots), \tag{3.2}$$

and this confirms the self-similar nature of slowly dissipating shallow-water solitary waves already noted by French (1969) and Hammack & Segur (1974).

Figure 6 shows the ξ, x trajectories (open symbols) for the interaction between the two waves corresponding to figure 4. Now we are in a position to account for the dissipation and the method proceeds as follows. First we define the 'interaction centre' (I.C.) as the x station where the vertical difference between the interacting trajectories is a minimum, and this is marked by the vertical line at x = 6·25 m for our example in figure 6. (In each experiment we found that the photographs which straddled the

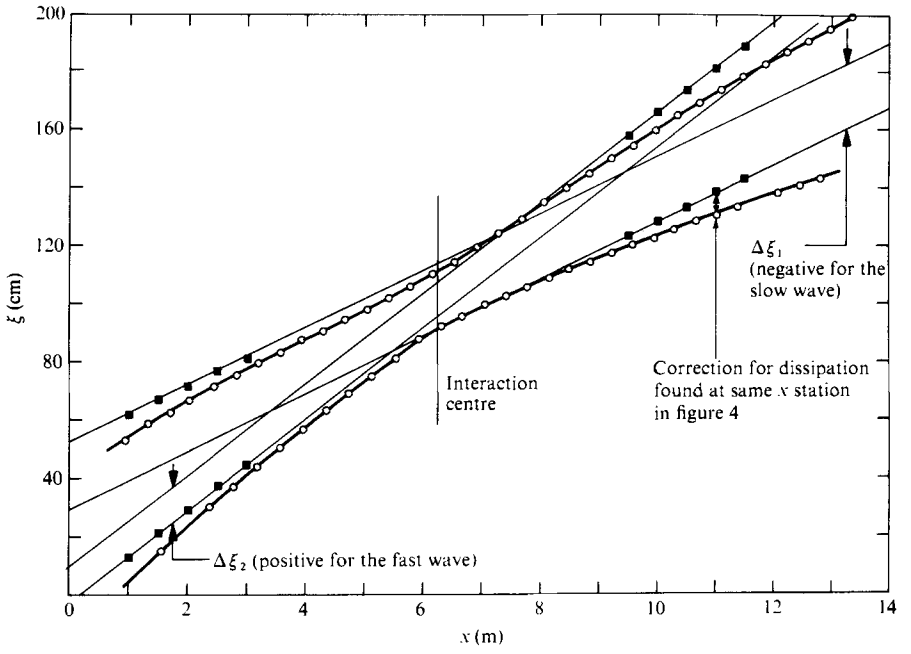

FIGURE 6. Interacting ξ, x trajectories (open circles) for the primary and secondary waves in the constant-width channel. Parallel lines are constructed through the data corrected for dissipation (solid squares). $\Delta\xi_1$ and $\Delta\xi_2$ are indicative of the spatial phase shifts. See text for details.

I.C. possessed the most symmetric wave forms, thus confirming that the I.C. defined here is essentially the middle of the interaction, as illustrated in figure 1.) Next, the tangents to the non-interacting ξ, x trajectories of each wave are drawn at the I.C., as shown in figure 4. Then the vertical deviations between the individual trajectories and their tangents (figure 4) are used to correct the interacting trajectories (figure 6) far from the I.C., where the interaction either has not yet started or is virtually complete. For those experiments in which the waves experience a complete interaction, asymptotic parallel lines can be constructed through the corrected data (solid squares), as indicated in figure 6. Knowing the slopes s_1 and s_2 of the asymptotes, one can recover the effective amplitudes α_1 and α_2 for the interaction by inverting (3.2) and using (3.1), viz.

$$\alpha_i = \tfrac{1}{6}\{10 - [100 - 240\, s_i/(1-s_i)]^{\frac{1}{2}}\}, \quad i = 1, 2. \tag{3.3}$$

For the example under consideration we have $s_1 = 0{\cdot}101$ and $s_2 = 0{\cdot}155$, which gives $\alpha_1 = 0{\cdot}242$ and $\alpha_2 = 0{\cdot}419$. Finally, the spatial phase shifts ΔX_1 and ΔX_2 are obtained by transforming the four asymptotic lines from the ξ, x plane to the ξ, t plane and measuring directly the ξ displacement between each pair of parallel lines. The results for this case are $\Delta X_1 = -24{\cdot}0$ cm for the slow wave and $\Delta X_2 = 14{\cdot}5$ cm for the fast wave. These measurements can then be compared with the theoretical non-dissipative spatial phase shifts calculated from the effective amplitudes using the equation (cf. Whitham 1974)

$$\Delta X_i = \mp \frac{h_0}{(3\alpha_i)^{\frac{1}{2}}} \ln\left(\frac{\sigma^{\frac{1}{2}}+1}{\sigma^{\frac{1}{2}}-1}\right)^2, \tag{3.4}$$

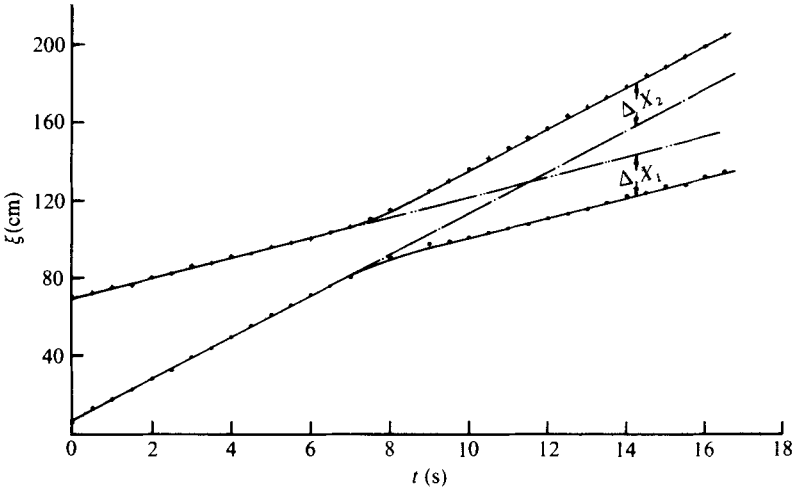

FIGURE 7. Interaction trajectories in the ξ, t plane for the converging channel. ΔX_1 and ΔX_2, measured between the parallel asymptotic trajectories, give the spatial phase shifts. See text for details.

where the ordered signs correspond to the indices $i = 1, 2$, respectively. Equation (3.4) yields $\Delta X_1 = -21{\cdot}1$ cm and $\Delta X_2 = 16{\cdot}0$ cm for our example.

3.2. *Wave propagation in a gradually converging channel*

As we have seen in the previous subsection, when a solitary wave propagates in a channel of constant width and depth its amplitude and wave speed decrease, while the volume of fluid represented by this decrease must be left behind as a small free-surface elevation. In order to compensate for this loss and maintain a more constant wave amplitude, two courses are open. The first of these is to decrease the fluid height, in a channel with a sloping bottom, but this has the undesirable effect of changing the zeroth-order wave speed $(gh_0)^{\frac{1}{2}}$. The second, to decrease the channel width in order to maintain the energy per unit width almost constant, is practical, can be justified *a priori* and can be validated *a posteriori*. Just as the solitary wave remains self-similar if the dissipation is small, so it must also do so if the convergence of the channel is so gradual that the basic nonlinear–dispersive balance is not upset.

In order to check these assumptions experimentally, the apparatus shown in figure 2 was modified by placing a second side wall at a slight angle to the other in such a way that the breadth of the channel varied linearly with downstream distance from 20·4 cm at the initial station to 8·1 cm at the 14 m station. The effectiveness of this scheme was realized in an almost constant amplitude propagation for the smaller waves, while the largest waves decreased in amplitude by no more than 10% over the entire length of the channel. In fact, for most cases the correction discussed in § 3.1, applied to these interacting trajectories, contributed an insignificant amount. One such case is displayed in an ξ, t diagram in figure 7. The phase shifts measured directly from this figure give $\Delta X_1 = -22$ cm and $\Delta X_2 = 21$ cm, while the corresponding theoretical phase shifts are $\Delta X_1 = -26$ cm and $\Delta X_2 = 18{\cdot}5$ cm.

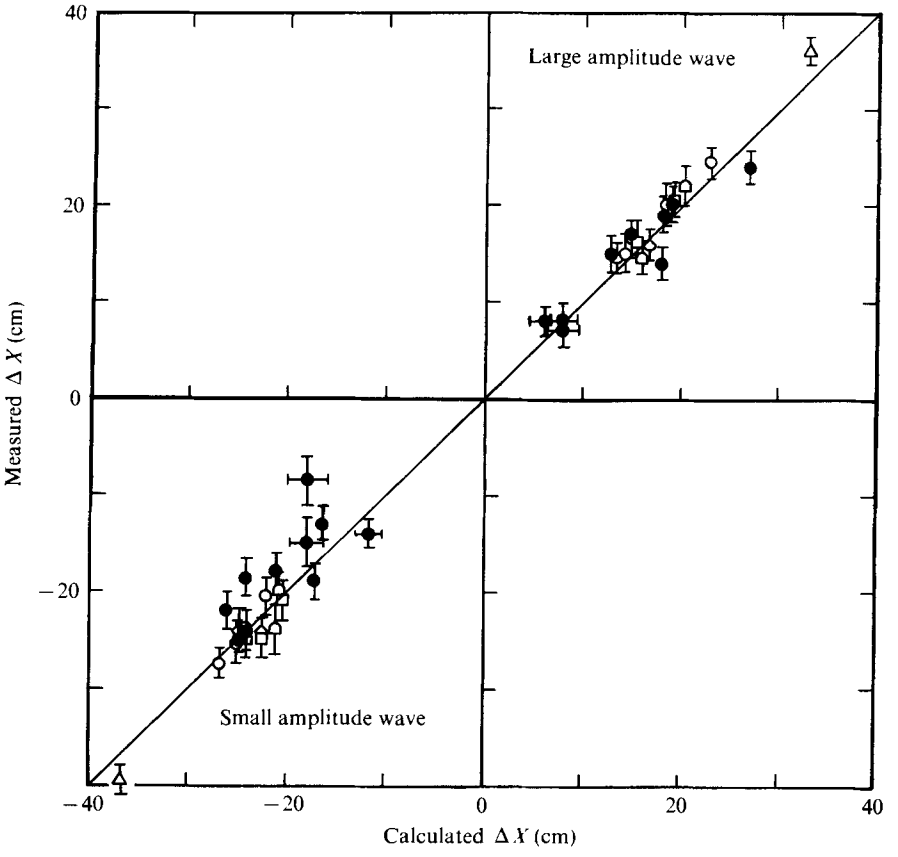

FIGURE 8. Comparison between the measured spatial phase shifts and those calculated using the effective amplitudes α_1 and α_2. ⊟, $h_0 = 4{\cdot}0$ cm; ⊟, $h_0 = 4{\cdot}5$ cm; ⊟, ●, $h_0 = 5{\cdot}0$ cm; ⊟, $h_0 = 5{\cdot}5$ cm; ⊟, $h_0 = 6{\cdot}0$ cm. The solid circles correspond to experiments performed in the converging channel.

4. Presentation of results

A series of interaction experiments covering the range $1{\cdot}2 < \sigma < 2{\cdot}7$ in the constant-width channel and the range $1{\cdot}6 < \sigma < 5{\cdot}0$ in the converging channel was performed. In the former, the still-water depth ranged from 4·0 cm to 6·0 cm and the estimates of the non-dissipative phase shifts were obtained by the method discussed in § 3.1. The experiments in the converging channel, on the other hand, all had a still-water depth of 5·0 cm and the spatial phase shifts were obtained directly from a plot of the ξ, t interaction trajectories. When necessary, a small adjustment of the asymptotic slopes about the I.C. was made to account for the slight wave attenuation. In both experiments the time delay between waves was set to locate the I.C. approximately at the mid-channel station so that sufficient data could be collected to determine the pre- and post-interaction trajectories unambiguously.

The data on the spatial phase shifts are presented in figure 8. Here we compare our measured results with the spatial phase shifts calculated from (3.4) using the effective wave amplitudes α_1 and α_2. The vertical error bars indicate the variations in measure-

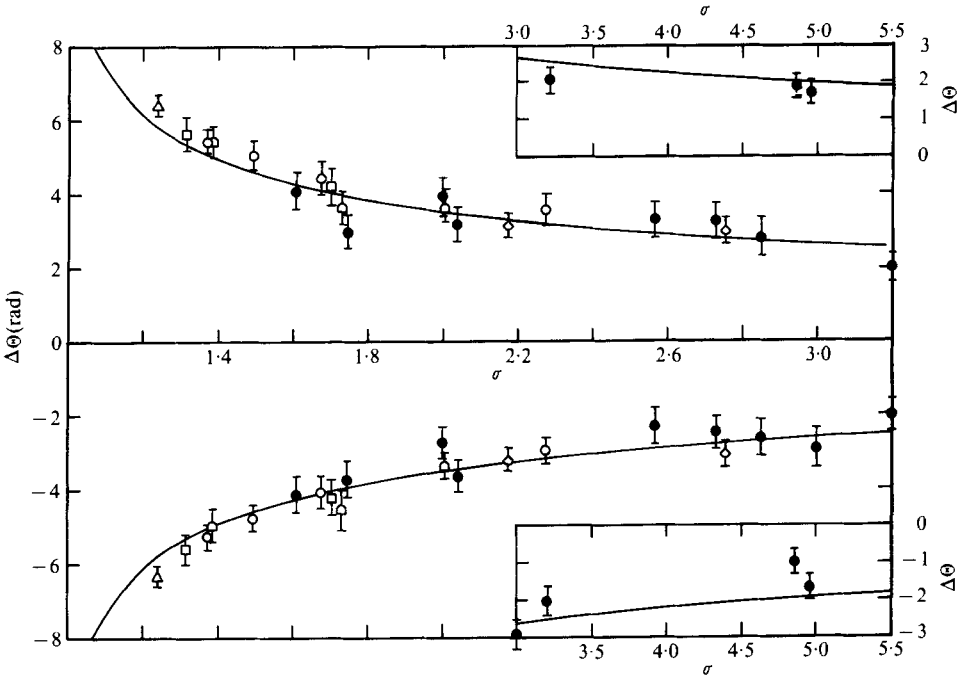

FIGURE 9. Angular phase shift as a function of the wave amplitude ratio. Solid lines correspond to the theoretical solution due to Hirota (1971). Symbols as in figure 8.

ments of the separation distance between the constructed parallel asymptotic trajectories. The data with horizontal error bars correspond to the largest measured amplitude ratios ($\sigma > 3$), and these error bars estimate the uncertainty in the amplitude measurements for the relatively small waves needed to achieve this condition. It is clear that, since the maximum amplitude for a stable solitary wave is $\alpha_2 \simeq 0{\cdot}7$ (see, for example, Laitone 1960), relatively large values of σ can be obtained only by decreasing the amplitude of the smaller, α_1 wave.

As an alternative presentation, we plot in figure 9 the 'angular' phase shift

$$\Delta\Theta_i = (3\alpha_i)^{\frac{1}{2}} \frac{\Delta X_i}{h_0} = \mp 2 \ln \left(\frac{\sigma^{\frac{1}{2}} + 1}{\sigma^{\frac{1}{2}} - 1} \right) \tag{4.1}$$

and note that theoretically it depends only on the amplitude ratio σ. The data from our two channels are in agreement in their region of overlap, $1{\cdot}6 < \sigma < 2{\cdot}7$, each lending support to the other as a viable method to account for the dissipation of the system. Both the spatial and the angular phase shift measurements in figures 8 and 9 are generally in good agreement with theory. We do note, however, some differences for the smaller wave for $\sigma > 3$. Our experience suggests that the photographic method of data acquisition becomes less reliable in tracking the crests of these relatively long flat waves, but this alone cannot entirely explain the observed discrepancies. (Phase shift measurements obtained using a string of electronic probes placed along the channel centre-line would help to resolve this problem.)

The photographs in figures 10 and 11 (plates 1 and 2) provide examples of the three types of KdV interaction discussed by Lax (1968). The waves are travelling from

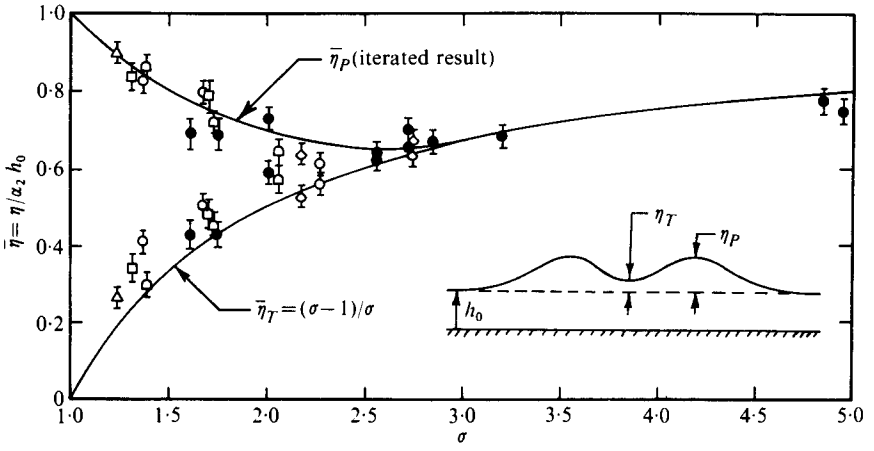

FIGURE 12. Mid-interaction amplitudes as a function of σ. Data points plotted one directly above the other for $\sigma < 3$ correspond to peak and trough amplitudes, respectively. The theoretical curves are derived from Hirota's (1971) exact solution. Symbols as in figure 8.

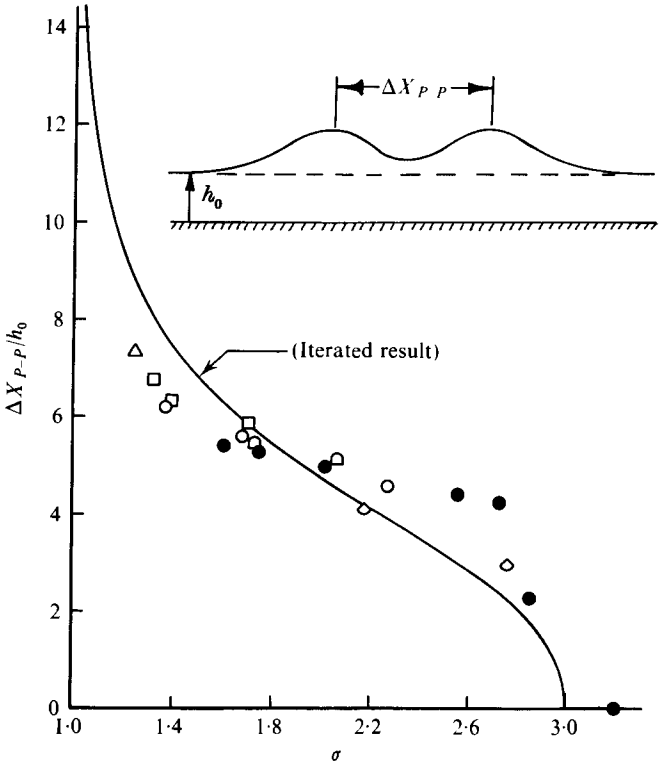

FIGURE 13. Separation distance between peaks at the middle of the interaction. The theoretical result obtained numerically from Hirota's (1971) solution is given by the solid line. Symbols as in figure 8.

right to left in each case and time increases vertically downwards. In figure 10 the exposures were taken at equal time intervals and are aligned to exhibit the forward and rearward phase shifts. Here $\sigma = 2{\cdot}04$, corresponding to case (*a*) in figure 1, where the peaks remain distinctly separate throughout the interaction. Exposures (*a*)–(*e*) in figure 11 are for $\sigma = 2{\cdot}56$, which is close to Lax's case (*b*) illustrated in figure 1. When figure 11 is viewed on edge to foreshorten the x co-ordinate, one can see that the small amplitude wave loses its crest in figures 11(*c*) and (*d*), but then regains it to form a symmetric double-crested wave form at the I.C. in figure 11(*e*). The short sequence in figures 11(*f*)–(*h*) for $\sigma = 4{\cdot}9$ is an example of Lax's case (*c*) interaction. Here the large amplitude wave completely overrides the smaller wave to form a single peak at the I.C. in figure 11(*h*).

Measurements characterizing the mid-interaction geometry have been obtained from the photographs exhibiting the most symmetric wave form in each interaction experiment (e.g. the middle frame in figure 10 and frames (*e*) and (*h*) in figure 11). Our experimental values of the peak amplitude η_P and trough amplitude η_T at the I.C. are compared with results derived from Hirota's (1971) solution in figure 12. One can readily show that the trough amplitude (which becomes the peak amplitude for $\sigma > 3$) is given by

$$\bar{\eta}_T = \eta_T/\alpha_2 h_0 = (\sigma - 1)/\sigma \tag{4.2}$$

while the peak amplitude in figure 12 was determined by an iteration procedure. The peak-to-peak distance ΔX_{P-P} between the wave crests at the I.C. has also been measured and is compared with the theoretical result in figure 13.

5. Summary and conclusion

Shallow-water wave experiments have been performed with the aim of testing Hirota's (1971) solution for the interaction of isolated solitons described by the KdV equation. Since the theory is inviscid, we have devised two methods of approximately correcting for dissipative effects, which, as pointed out in the appendix, were particularly important for waves propagating on the shallow fluid layers in our relatively narrow Plexiglas channel. For the constant-width channel we have used the measured amplitude decay of the individual, non-interacting waves to correct their asymptotic interaction trajectories. In the second method, we have allowed the channel walls to converge slightly in such a way as to maintain an almost constant amplitude propagation of the individual waves. Application of these corrective measures gives rise to 'effective' wave amplitudes which characterize the interaction and provide the basis for comparison with theory.

We have already noted the agreement in figure 9 between the angular phase shift measurements obtained from our two compensation techniques. Within experimental error we also note substantial agreement with the theoretical logarithmic curve over a large range of σ. The success of our tedious correction described in § 3.1 is not so surprising when one remembers that the fore and aft angular phase shifts depend only on the ratio of the wave amplitudes. Thus, although the dissipation may be large over the distances necessary to complete an interaction, each wave suffers a comparable degradation such that the variation in σ is small. The spatial phase shifts in figure 8, on the other hand, as well as the peak and trough amplitudes in figure 12, depend on

the actual wave amplitudes, and this explains the increased scatter found in these data.

The amplitude error bars in figure 12 do not include estimates of the meniscus effect at the side wall, and we have implicitly assumed that the effective amplitude ratio in figures 12 and 13 represents the true (but unknown) instantaneous value at the I.C. In spite of these shortcomings, the measured characteristics of the mid-interaction wave-form geometry are seen to exhibit the expected theoretical trends.

In conclusion, the experimental results provide good qualitative as well as quantitative agreement with KdV theory for collisions between two solitary waves propagating in the same direction. We have been able to produce each of the three interactions discussed by Lax (1968) and it is satisfying that we can actually discern a class (*b*) type of interaction. Most of the observed differences between theory and experiment can be attributed, at least in part, to our averaging technique, which was necessary in order to make meaningful comparisons with Hirota's (1971) solution. However, we cannot rule out the possible need for higher-order theoretical corrections since some of the effective amplitudes in our experiment approached a value of 0·5.

We are grateful to our colleague Larry Redekopp for helpful discussions throughout the course of this experiment. We also recognize and appreciate the assistance of our laboratory technician, Casey de Vries. The electronic circuit controlling the wave maker was designed and built by Tim Jentes. This work was supported by the National Aeronautics and Space Administration, Planetary Atmospheres Branch, under grant NGR-05-018-178.

Appendix

This section is provided to address some questions of general interest raised by the referees of this paper concerning our dissipation measurements. In particular, we endeavour to explain apparent discrepancies between our measurements and those of prior investigators, which are sometimes in agreement with Keulegan's (1948) theory.

Keulegan's analysis combines the nonlinear aspects of small amplitude solitary waves with linearized laminar boundary-layer theory. A simple wetted-surface approximation is used to account for side-wall dissipation without regard for the wetted surface of the wave itself. Keulegan has not attempted to model the viscous dissipation at the free surface caused by contamination and surface-tension effects, nor has he considered the problem of capillary hysteresis mentioned in § 3. Nonetheless, Keulegan's inverse fourth-power law has been used as a guideline for this by and large unresolved problem. Several authors have since rederived the inverse fourth-power law with some variation in the proportionality constant (e.g. Iwasa 1959), and the most recent exposition is probably that due to Miles (1977*a*). From the above considerations, one would perhaps expect Keulegan's theory to overpredict the wave amplitudes since his analysis neglects dissipation mechanisms which may be of considerable importance. We shall not attempt to analyse all the possible contributing factors, but a comparison of our measurements with prior experimental work is worthwhile.

The amplitudes measured in our facility are as much as 15% (at $h_0 = 8{\cdot}1$ cm),

25% (at $h_0 = 5{\cdot}0$ cm) and 40% (at $h_0 = 4{\cdot}0$ cm) smaller than those predicted (see figure 3). Dissipation measurements have also been reported by Ippen, Kulin & Raza (1955), French (1969) and Hammack & Segur (1974). French compares his measurements with those of Ippen *et al.* in figure 6.11 of his report. The combined measurements show amplitudes ranging from 4% above (8 data points) to 18% below (38 data points) Keulegan's prediction. Moreover, while about half of the data (generally at large fluid depths, $h_0 \geqslant 15$ cm) can be considered to agree with the theory, the remaining half of the data (generally at small fluid depths, $h_0 < 15$ cm) represents dissipations considerably in excess of those predicted by Keulegan. The largest discrepancies are reported at depths of 9 cm and 12 cm, only slightly larger than the depths

$$4 \text{ cm} < h_0 < 8 \text{ cm}$$

used in the present experiment. It is also evident that the relatively large scatter in these data cannot be accounted for by a simple change in Keulegan's proportionality constant. Hammack & Segur, on the other hand, present results (at $h_0 = 5{\cdot}0$ cm) which can be used to infer that the amplitudes of the leading solitons which emerge from their initial disturbances are 5–20% greater than Keulegan's prediction, in contradiction to the results cited above for only slightly larger fluid depths. One must be careful to realize, however, that no direct measurements for an isolated solitary wave were reported by Hammack & Segur, and for this reason their results can be only suggestive of dissipation trends.

Capillary hysteresis may have contributed measurably to the decay of solitary waves in our Plexiglas channel and also in the lucite channel used by Ippen *et al.* The production of capillary waves at the side walls is a manifestation of energy lost from the main wave, but there may be other, less obvious frictional effects which critically depend on conditions at the air–water–lucite contact line. Experiments performed by Keulegan (1959), for example, show that the dissipation of standing waves in a lucite basin is 'much greater in comparison to that in a glass basin', and the investigation by Miles (1967) supports the idea that this result is due to capillary hysteresis. There is no evidence which suggests that these effects can be neglected for free-surface waves propagating in rectangular channels.

We see that the dissipation of solitary waves in a rectangular channel is a difficult and as yet unresolved problem. Carefully controlled experiments are needed to determine the relative importance of the various dissipative mechanisms. This information can then be used to motivate future analytical studies and may also provide a basis of comparison for results obtained in different experimental facilities.

REFERENCES

BYATT-SMITH, J. G. B. 1971 An integral equation for unsteady surface waves and a comment on the Boussinesq equation. *J. Fluid Mech.* **49**, 625–633.

FRENCH, J. A. 1969 Wave uplift pressures on horizontal platforms. *Calif. Inst. Tech., Pasadena Rep.* KH-R-19.

HAMMACK, J. L. & SEGUR, H. 1974 The Korteweg–de Vries equation and water waves. Part 2. Comparison with experiments. *J. Fluid Mech.* **65**, 289–314.

HIROTA, R. 1971 Exact solution of the Korteweg–de Vries equation for multiple collisions of solitons. *Phys. Rev. Lett.* **27**, 1192–1194.

IPPEN, A. T., KULIN, G. & RAZA, M. A. 1955 Damping characteristics of the solitary wave. *Hydrodyn. Lab., M.I.T. Tech. Rep.* no. 16.

IWASA, Y. 1959 Attenuation of solitary waves on a smooth bed. *A.S.C.E. Trans.* **24**, 193–206.

KEULEGAN, G. H. 1948 Gradual damping of solitary waves. *Nat. Bur. Sci. J. Res.* **40**, 487–498.

KEULEGAN, G. H. 1959 Energy dissipation in standing waves in rectangular basins. *J. Fluid Mech.* **6**, 33–50.

KRUSKAL, M. D. 1974 The Korteweg–de Vries equation and related evolution equations. *Lectures in Appl. Math.* vol. 15. *Nonlinear Wave Motion*, pp. 61–83.

LAITONE, E. V. 1960 The second approximation to cnoidal and solitary waves. *J. Fluid Mech.* **9**, 430–444.

MAXWORTHY, T. 1976 Experiments on collisions between solitary waves. *J. Fluid Mech.* **76**, 177–185.

MILES, J. W. 1967 Surface-wave damping in closed basins. *Proc. Roy. Soc.* A **297**, 459–475.

MILES, J. W. 1977*a* Damping of weakly nonlinear shallow-water waves. *J. Fluid Mech.* **76**, 251–257.

MILES, J. W. 1977*b* Obliquely interacting solitary waves. *J. Fluid Mech.* **79**, 157–169.

OIKAWA, M. & YAJIMA, N. 1973 Interactions of solitary waves – a perturbation approach to non-linear systems. *J. Phys. Soc. Japan* **34**, 1093–1099.

WHITHAM, G. B. 1974 *Linear and Non-Linear Waves.* Interscience.

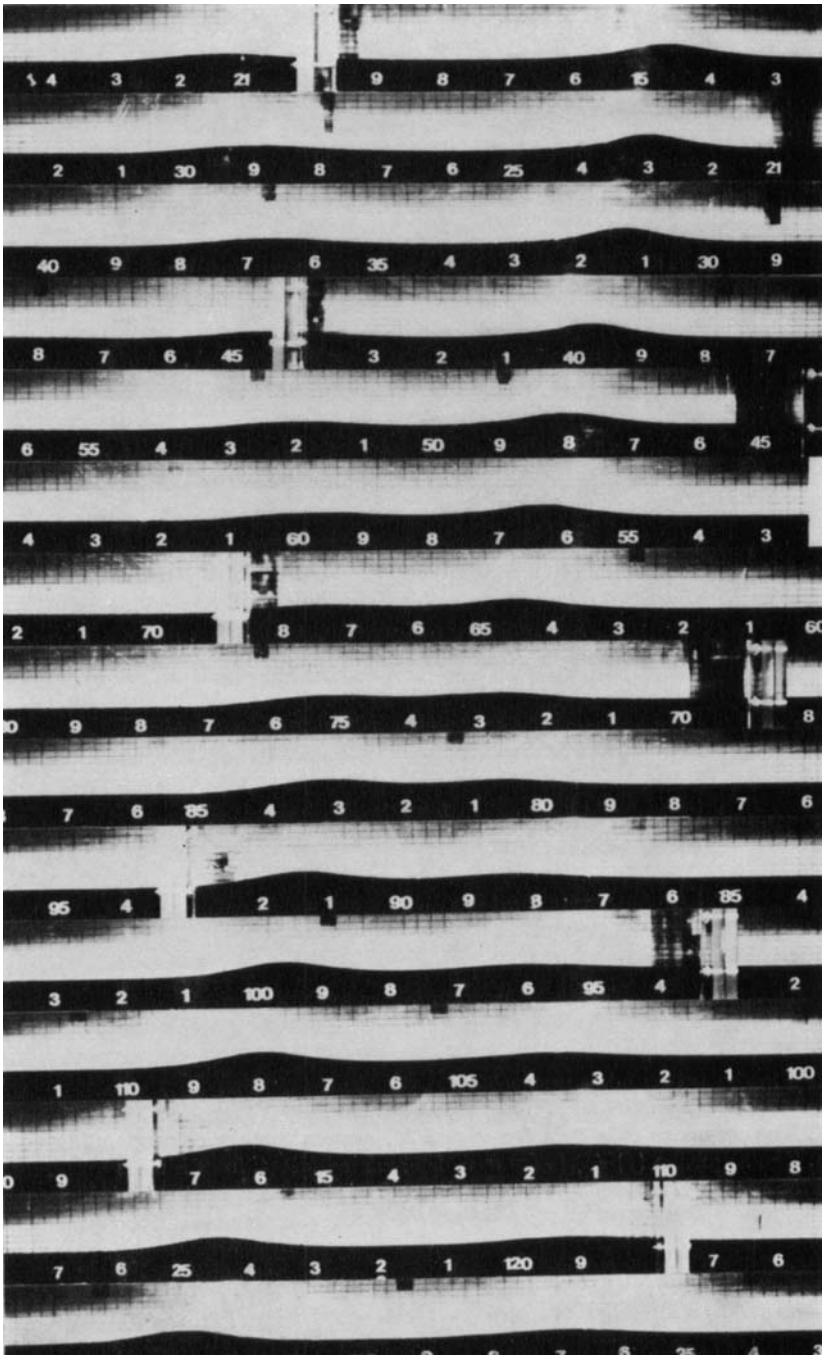

FIGURE 10. Photographic sequence exhibiting a class (*a*) interaction for $\sigma = 2{\cdot}04$. The waves propagate from right to left and time increases downwards at 1·0 s intervals.

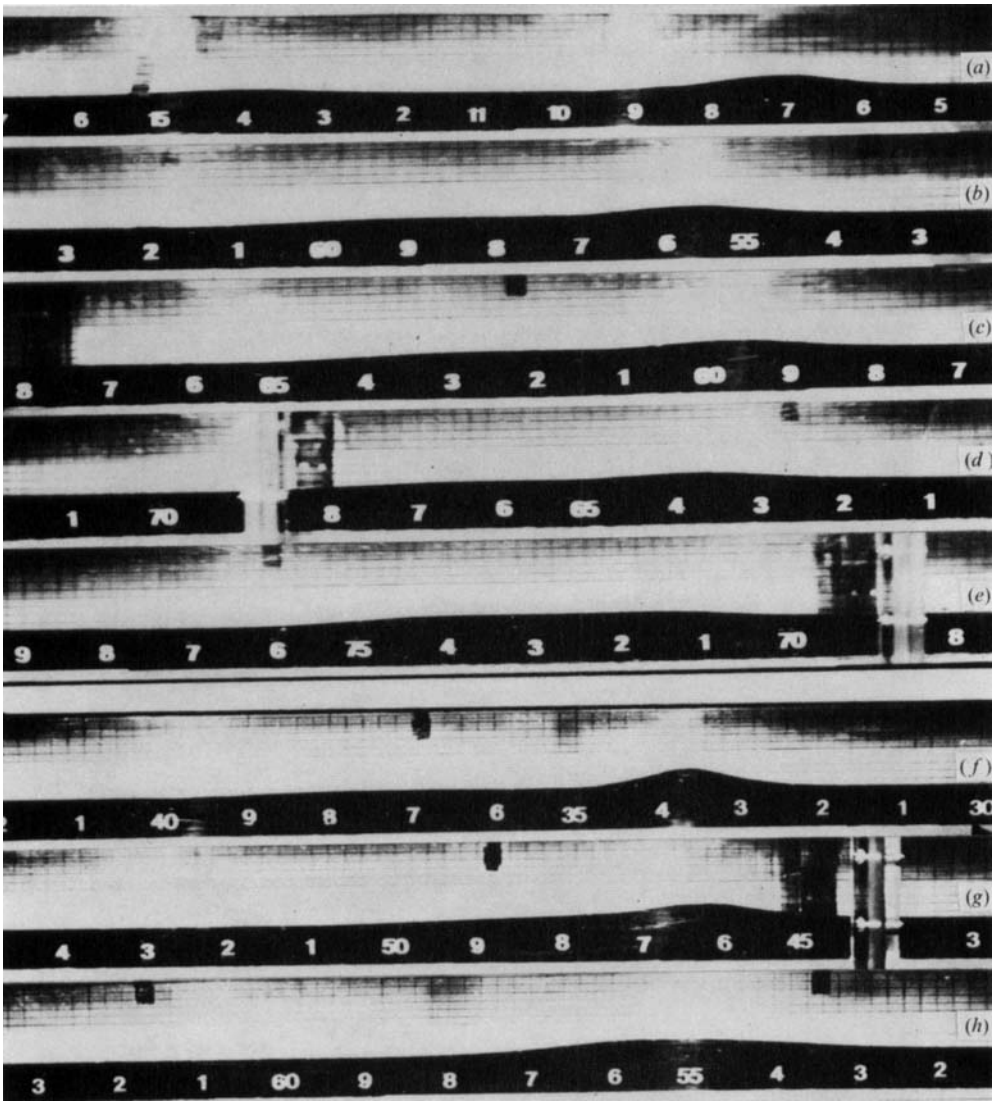

FIGURE 11. The sequence (*a*)–(*e*) is for $\sigma = 2{\cdot}56$, approximately corresponding to a class (*b*) interaction. The sequence (*f*)–(*h*) is for $\sigma = 4{\cdot}9$ and is indicative of a class (*c*) interaction. The last photograph in each sequence corresponds to the interaction centre (I. C.).